ChemComm

COMMUNICATION

View Article Online
View Journal | View Issue

Cite this: *Chem. Commun.*, 2025, **61**, 7301

Received 11th March 2025,
Accepted 10th April 2025

DOI: 10.1039/d5cc01314c

rsc.li/chemcomm

A facile one-pot recipe for topological insulator Bi_2Se_3 with thermoelectric properties†

Anil Kumar B. M.,[a] Rittika Dhar,[a] Shuva Biswas[b] and Satya N. Guin *[a]

Topological materials from heavy p-block metal chalcogenides with layered structures and anisotropic bonding are of immense importance for thermoelectrics. The synthesis of such materials with simple chemical routes is of high significance. Here, we present a low-temperature, facile, one-pot, and cost-effective synthesis of topological insulator Bi_2Se_3 nanosheets. The material demonstrates excellent electrical transport and low thermal conductivity, leading to a peak thermoelectric figure of merit (*ZT*) of ~0.41 at 480 K. Additionally, the synthesis of Bi_2S_3 nanoparticles under ambient conditions suggests the versatility of the method.

Materials with strong chemical bonding in the in-plane direction and weak van der Waals interlayer type (*e.g.* SnSe, MoS_2, WS_2, Bi_2Te_3) or weak electrostatic interactions (*e.g.* BiCuSeO, Bi_2O_2Se, BiAgOS) along the stacking direction are called two-dimensional (2D) materials. After the graphene surge, there has been significant activity in the synthesis of non-carbon-based inorganic solid-state 2D materials. This is driven by their promising applications and the need for a deeper understanding of structure–property relationships.[1–4] The high surface-to-volume ratio of these nanostructured 2D materials, coupled with the quantum confinement effect of charge carriers in two dimensions, gives rise to a range of fascinating properties and potential applications in fields such as electronics,[3,5] catalysis,[6,7] energy storage,[3,8] and energy conversion.[4,9]

In recent years, topological materials, a class of quantum materials, have earned widespread interest. These materials have become the focal point of research due to their remarkable potential for various applications, including thermoelectrics, quantum computing, and catalysis.[10–14] The demand for similar material characteristics like heavy elements and small band gaps highlights the strong connection between the topological electronic structure and thermoelectrics.[12] For instance, Bi_2Se_3 is known for its promising thermoelectric properties. In addition to its narrow band gap, the fascination with Bi_2Se_3 also comes from its topological insulator (TI) nature due to spin–orbit coupling. In the bulk of TIs, the valence and conduction bands are separated by a band gap, while at the surface, the valence and conduction bands are linked by metallic topological surface states.[11,15–17] These exotic topologically protected surface states were observed experimentally using angle-resolved photoemission spectroscopy (ARPES) experiments, and the topological signature has been verified in transport measurements.[18,19] The effect of topological surface states in transport decreases with increasing number of layers in TIs as the contribution of bulk states plays a dominant role. Therefore, atomically thin few layer Bi_2Se_3 is promising for thermoelectrics due to its enhanced topologically protected surface states, which results in excellent charge transport.

Traditionally, high-temperature solid-state, chemical and vapour deposition methods and molecular beam epitaxy have been employed to yield TIs with a few to ~30 quintuple layer (QL) thickness. The need for a facile route to synthesise few QL Bi_2Se_3 has attracted significant attention in solution phase synthesis. Mechanical exfoliation,[16] ionothermal synthesis,[20] the polyol method,[21–23] vapour–solid synthesis,[24] molecular beam epitaxy[25] and chemical vapour transport[26] have been employed to synthesize few-layer Bi_2Se_3. Often, these methods are limited by complicated reaction setups, expensive reagents, and toxic by-products. Therefore, a facile, scalable, and environmentally friendly synthetic route is still of great interest to explore. Recently, a simple route for obtaining Se activation by ethanolamine and the synthesis of various metal chalcogenides such as Ag_2Se, FeSe, and CdSe has been demonstrated without hazardous side products.[27,28]

Herein, we report a simple, low cost, environmentally friendly synthesis of few layered Bi_2Se_3 nanosheets. We have found that the ethanolamine-mediated synthesis reaction of bismuth neodecanoate and SeO_2 yields few QL Bi_2Se_3

[a] *Department of Chemistry, Birla Institute of Technology and Science, Pilani, Hyderabad Campus, Jawahar Nagar, Hyderabad 500078, India. E-mail: satyanarayan.g@hyderabad.bits-pilani.ac.in*
[b] *New Chemistry Unit, Jawaharlal Nehru Centre for Advanced Scientific Research (JNCASR), Jakkur P. O., Bengaluru 560064, India*

† Electronic supplementary information (ESI) available. See DOI: https://doi.org/10.1039/d5cc01314c

nanostructures at 160 °C. We have used powder X-ray diffraction (PXRD), field emission scanning electron microscopy (FESEM), and transmission electron microscopy (TEM) for the characterization of the materials. FESEM and TEM studies reveal the few-layer nature of the nanosheets. The synthesized Bi_2Se_3 nanostructures were explored for electronic and phonon transport properties. The Bi_2Se_3 nanosheets exhibit excellent charge transport properties and low thermal conductivity. A peak promising thermoelectric figure of merit $ZT \sim 0.41$ at 480 K was achieved, which is comparable to reported Bi_2Se_3 and provides practical relevance. We also demonstrate that ethanolamine-mediated synthesis produces Bi_2S_3 under ambient conditions, highlighting the versatility and generality of the method.

Bi_2Se_3 crystallizes in an anisotropic layered structure with $R\bar{3}m$ space group. The structure contains quintuple layers (QLs) of five covalently bonded [Se_2–Bi–Se_1–Bi–Se_2] atomic planes each of approximately 1 nm thickness. These QLs are periodically aligned along the crystallographic *c*-axis by weak van der Waals-like interactions (Fig. 1a).[15,20,21,29] In a typical one-pot synthesis, Bi neodecanoate and SeO_2 were used as metal and Se sources, respectively. Ethanolamine (2-amino-1-ethanol) was used as both a solvent and a soft reducing agent to reduce Se^{4+} to Se^{2-} to facilitate the reaction with Bi^{3+} to yield a few quintuple layer Bi_2Se_3 nanosheets. The reaction was performed at a temperature of 160 °C for 30 minutes under normal atmospheric conditions. The reaction mixture was allowed to cool naturally, after which the Bi_2Se_3 nanosheets were collected through sequential washing and drying.

PXRD patterns of the as-synthesized Bi_2Se_3 samples can be indexed based on a rhombohedral structure with an $R\bar{3}m$ space group (Fig. 1b).[20,23] The sharp nature of the peaks indicates the high crystalline nature of the material. In contrast, a similar approach to synthesise Bi_2S_3 under ambient conditions results in broad peaks (Fig. S1a, ESI†), which could be attributable to the small size of the particles (Fig. S2a and b, ESI†). The crystallinity of the synthesized Bi_2S_3 was improved following annealing at 573 K in a vacuum-sealed tube (Fig. S1a, ESI†). Efforts to synthesise Bi_2Te_3 have yielded Bi_2Te_3 with elemental tellurium as an impurity (Fig. S7, ESI†), probably due to the low reactivity of tellurium.

In order to understand the morphology and elemental composition of Bi_2Se_3, FESEM coupled with energy dispersive X-ray analysis (EDX) was performed. The FESEM (Fig. 2a and b) images indicate the ultrathin nature of the Bi_2Se_3 nanosheets. The EDX analysis shows the appropriate stoichiometry ratio of the consistent elements (Fig. 2f). Moreover, the uniform distribution of Bi and Se is confirmed by the elemental colour mapping (Fig. 2c–e) indicating the single-phase homogeneity of Bi_2Se_3 nanosheets. The formation of ultrathin nanosheets is further confirmed by the TEM (Fig. 3a and Fig. S4, ESI†) images. The high-resolution TEM (Fig. 3b) shows a distinct lattice spacing of ~4.7 Å corresponding to the (006) interplanar distance. The selected-area electron diffraction (SAED) pattern obtained from a single sheet region reveals the single-crystal nature of the nanosheets (inset of Fig. 3b).

The X-ray photoelectron spectroscopy (XPS) of the as-synthesized Bi_2Se_3 nanosheets was performed to understand the presence of constituent elements and their oxidation states. Two sharp peaks at ~162.78 eV and ~157.48 eV correspond to

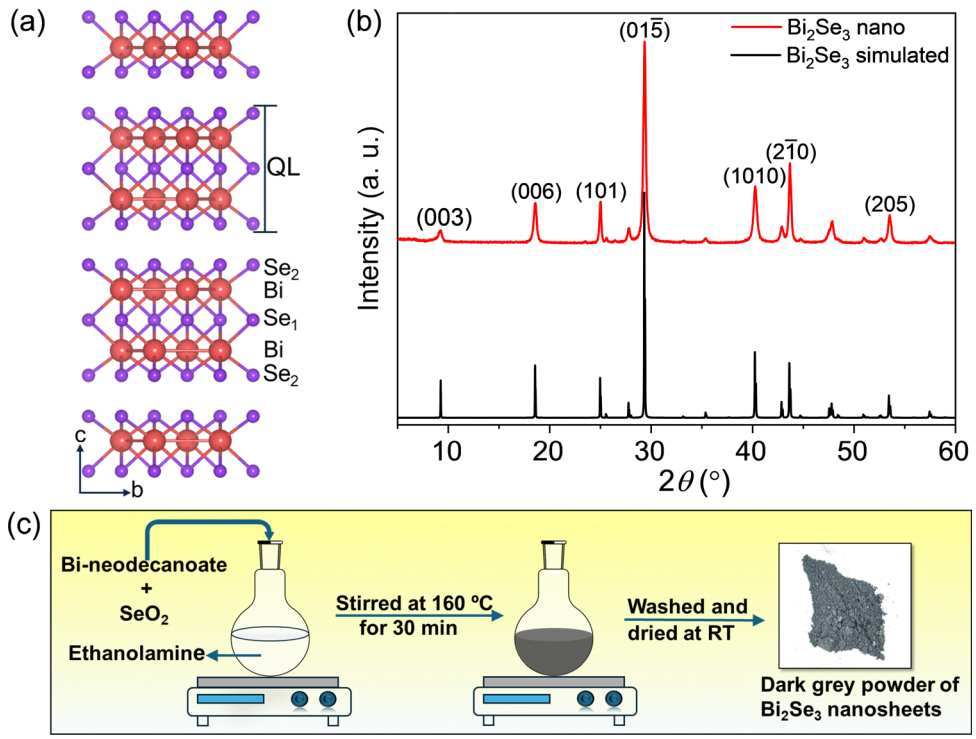

Fig. 1 (a) Crystal structure of Bi_2Se_3 viewed down the crystallographic axis *a*, (b) room temperature PXRD pattern of the Bi_2Se_3 nanosheets with the simulated pattern (COD: 00-901-1965), and (c) a schematic representation of a Bi_2Se_3 nanosheet synthesis process.

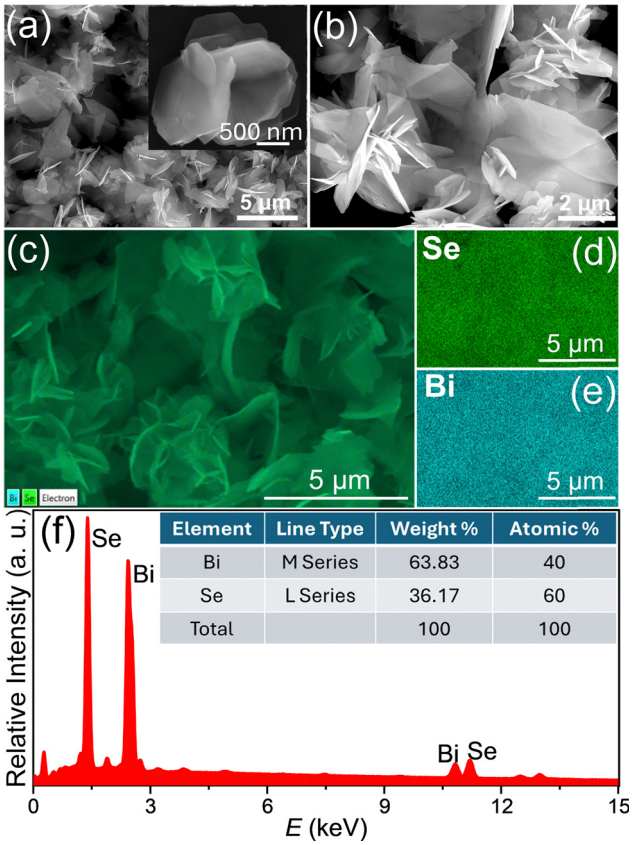

Element	Line Type	Weight %	Atomic %
Bi	M Series	63.83	40
Se	L Series	36.17	60
Total		100	100

Fig. 2 (a) and (b) Typical FESEM images of Bi_2Se_3 nanosheets. (c)–(e) EDX elemental colour mapping of Bi_2Se_3 nanosheets. A homogenous distribution of Bi and Se is observed in the Bi_2Se_3 nanosheets. (f) EDX spectra of the as-synthesized Bi_2Se_3; the inset table shows the corresponding elemental composition.

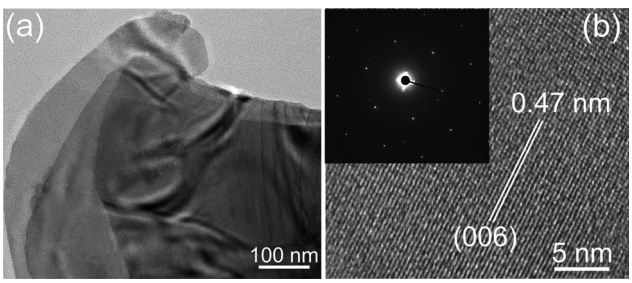

Fig. 3 (a) A typical low magnification TEM image of Bi_2Se_3 nanosheets showing stacking of the nanosheets and (b) HRTEM image showing the (006) lattice planes of the Bi_2Se_3 nanosheets. Inset with the corresponding SAED pattern from a single sheet region of Bi_2Se_3.

the spin–orbit coupled peaks of Bi $4f_{5/2}$ and Bi $4f_{7/2}$, respectively (Fig. 4a), which is consistent with the Bi(III), and the peaks at ~53.85 eV and ~52.98 eV are attributed to Se $3d_{3/2}$ and Se $3d_{5/2}$, suggesting the purity of the phase (Fig. 4b).[17,29] The peaks were fitted using a Gaussian model, with excellent goodness of fit (R^2) values of 0.994 for Bi and 0.996 for Se. The XPS analysis of the synthesized Bi_2S_3 sample reveals the presence of its constituent elements, with peak positions closely matching those reported in the literature (Fig. S6, ESI†).

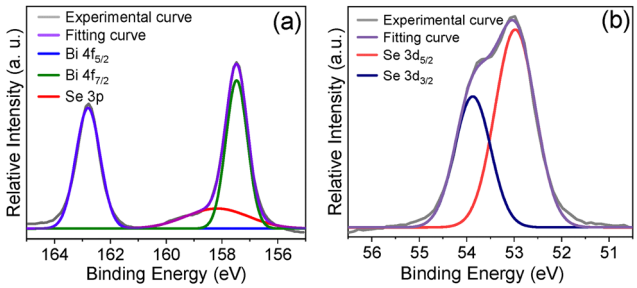

Fig. 4 X-ray photon electron spectra of the Bi_2Se_3 nanosheets. (a) Bi 4f exhibiting a peak splitting of ~5.4 eV corresponding to Bi(III) and (b) Se 3d suggesting the purity of the phase.

The presence of heavy elements, anisotropic layered structure and TI nature of Bi_2Se_3 motivated us to investigate the electrical and thermal properties of the as-synthesized nanosheets. To measure the transport properties of the Bi_2Se_3 nanosheets, first, we have performed hydrazine treatment (see experimental section, ESI†) to remove any surface adsorbed ligands. The sample was densified by employing a hot press at 748 K for 30 minutes under 50 MPa pressure. The density of the pressed sample is ~7.043 g cm^{-3} (~92% theoretical density). To understand the effect of hot pressing on the nanosheets, PXRD and FESEM imaging were done. The PXRD pattern of the crushed pellet displays a good agreement with the simulated pattern (Fig. S8a, ESI†), Backscattered mode FESEM imaging (Fig. S8c, ESI†) confirms the retention of a single phase. FESEM imaging of the fractured pellet surface shows the retention of the few layered nature of the Bi_2Se_3 nanosheets (Fig. S8b, ESI†). Moreover, the EDX composition and elemental colour mapping analysis show the appropriate stoichiometry ratio and uniform distribution of Bi and Se in the hot-pressed sample (Fig. S9, ESI†).

In Fig. 5, we show the optical images and thermoelectric transport data for the Bi_2Se_3 sample. The electrical and thermal transport properties are measured along the hot pressing direction (∥ to hot pressed) (Fig. 5a and b). The electrical conductivity (σ) of the sample increases with temperature, rising from ~219 S cm^{-1} at 335 K to ~291 S cm^{-1} at 725 K (Fig. 5c). The negative Seebeck coefficient indicates a n-type conduction in the sample with a measured S value of ~−121 μV K^{-1} at 335 K, which shows a peak value of ~−131 μV K^{-1} at 481 K and then it reaches a value of ~−119 μV K^{-1} at 725 K (Fig. 5d). A similar trend in Seebeck value was observed previously in few QL Bi_2Se_3.[21]

Thermal conductivity (κ) was calculated using the relation $\kappa = DC_p\rho$, where D is thermal diffusivity, C_p is specific heat capacity, and ρ is the density of the material (see Fig. S10, ESI†). Thermal conductivity of the as-synthesized materials ranges from ~0.4 W m^{-1} K^{-1} at 296 K to ~0.75 W m^{-1} K^{-1} at 725 K (Fig. 5e). The lattice thermal conductivity, κ_{lat}, was obtained by subtracting the electronic part of the thermal conductivity, κ_e, from the κ_{total} utilising the Wiedemann–Franz law, $\kappa_e = L\sigma T$, where L is Lorenz number, and T is temperature. The estimation indicates that the nanosheets exhibit ultralow lattice thermal conductivity (Fig. S11a, ESI†). This low thermal conductivity arises due to phonon scattering at the surface and

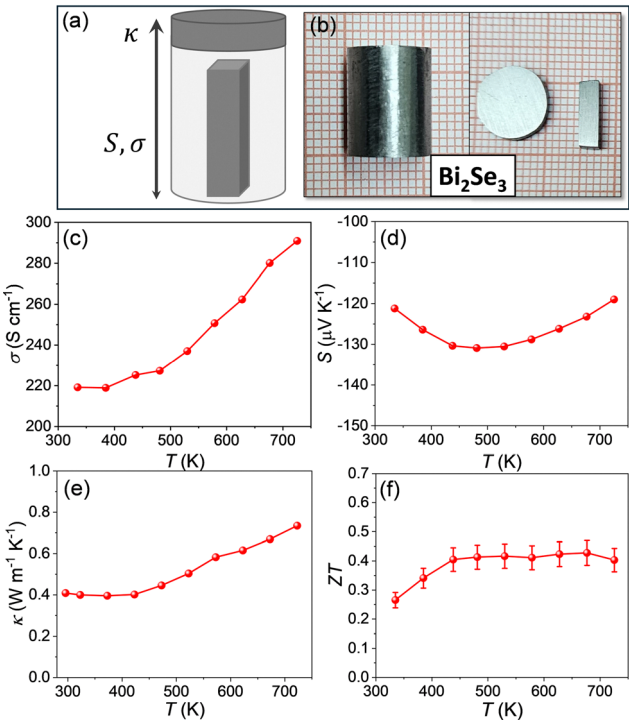

Fig. 5 (a) Schematic representation of a cylinder with the sample cut along the hot pressing direction for thermal and electrical transport measurements. (b) Images of a hot-pressed cylinder, which was further cut into a coin and bar-shape for the thermoelectric property measurements. Temperature dependent (c) electrical conductivity (σ), (d) Seebeck coefficient (S), (e) thermal conductivity (κ), and (f) thermoelectric figure of merit (ZT) of the Bi_2Se_3 nanosheets. A 10% error bar is shown for ZT estimation.

layer interface and the presence of low-energy optical phonon modes, which usually scatter the heat-carrying acoustic phonons. From the electrical conductivity and Seebeck data, a maximum power factor of $\sim$4.25 μW cm^{-1} K^{-2} is estimated at 675 K (Fig. S11b, ESI†). The peak thermoelectric figure of merit (ZT) value is estimated to be $\sim$0.41 at 480 K (Fig. 5f). It must be mentioned that the ZT value of the as-synthesized sample is comparable to previously reported Bi_2Se_3 (Table S1, ESI†). This finding implies that the described one-pot synthesis approach effectively produces high-quality materials.

In conclusion, we have successfully demonstrated a one-pot synthesis route of Bi_2Se_3 using Bi neodecanoate and SeO_2 in 2-amino-1-ethanol solvent. Utilizing the present method, we also synthesized Bi_2S_3 nanoparticles under ambient conditions. The technique employs a very simple, capping-agent-free and scalable approach. The Bi_2Se_3 nanosheets exhibit promising charge transport properties. The layered structure and nano/meso-scale interfaces cause significant phonon scattering, which results in low thermal conductivity and a promising ZT. The simplicity of the current synthetic method, along with the promising transport properties, paves the way for environmentally friendly synthesis of multifunctional materials.

This work is supported by the Core Research Grant (CRG) (CRG/2022/004125), Anusandhan National Research Foundation (ANRF), Govt. of India and New Faculty Seed Grant, BITS Pilani. A. K. B. M. and R. D. thank BITS Pilani and ANRF, respectively, for a PhD fellowship. S. B. acknowledges JNCASR for the fellowship. The authors also acknowledge the central analytical facilities of BITS Pilani, Hyderabad Campus for providing facilities.

Data availability

The data supporting this article have been included in the references and the ESI.†

Conflicts of interest

There are no conflicts to declare.

Notes and references

1 K. S. Novoselov, V. I. Falko, L. Colombo, P. R. Gellert, M. G. Schwab and K. Kim, *Nature*, 2012, **490**, 192–200.
2 K. S. Novoselov, A. Mishchenko, A. Carvalho and A. H. Castro Neto, *Science*, 2016, **353**, aac9439.
3 M. Chhowalla, H. S. Shin, G. Eda, L.-J. Li, K. P. Loh and H. Zhang, *Nat. Chem.*, 2013, **5**, 263–275.
4 M. Samanta, T. Ghosh, S. Chandra and K. Biswas, *J. Mater. Chem. A*, 2020, **8**, 12226–12261.
5 B. Radisavljevic, M. B. Whitwick and A. Kis, *ACS Nano*, 2011, **5**, 9934–9938.
6 G. Li, Q. Xu, W. Shi, C. Fu, L. Jiao, M. E. Kamminga, M. Yu, H. Tüysüz, N. Kumar, V. Süß, R. Saha, A. K. Srivastava, S. Wirth, G. Auffermann, J. Gooth, S. Parkin, Y. Sun, E. Liu and C. Felser, *Sci. Adv.*, 2019, **5**, eaaw9867.
7 X. Kong, Z. Liu, Z. Geng, A. Zhang, Z. Guo, S. Cui, C. Xia, S. Tan, S. Zhou, Z. Wang and J. Zeng, *J. Am. Chem. Soc.*, 2024, **146**, 6536–6543.
8 K. Chang and W. Chen, *Chem. Commun.*, 2011, **47**, 4252.
9 L. D. Zhao, S. H. Lo, Y. Zhang, H. Sun, G. Tan, C. Uher, C. Wolverton, V. P. Dravid and M. G. Kanatzidis, *Nature*, 2014, **508**, 373–377.
10 B. Bradlyn, L. Elcoro, J. Cano, M. G. Vergniory, Z. Wang, C. Felser, M. I. Aroyo and B. A. Bernevig, *Nature*, 2017, **547**, 298–305.
11 N. Kumar, S. N. Guin, K. Manna, C. Shekhar and C. Felser, *Chem. Rev.*, 2021, **121**, 2780–2815.
12 Y. Pan, B. He, X. Feng, F. Li, D. Chen, U. Burkhardt and C. Felser, *Nat. Mater.*, 2025, **24**, 76–82.
13 A. Kumar and S. N. Guin, *Mater. Chem. Front.*, 2023, **7**, 4202–4214.
14 C. Fu, Y. Sun and C. Felser, *APL Mater.*, 2020, **8**, 040913.
15 H. Zhang, C.-X. Liu, X.-L. Qi, X. Dai, Z. Fang and S.-C. Zhang, *Nat. Phys.*, 2009, **5**, 438–442.
16 S. Y. F. Zhao, C. Beekman, L. J. Sandilands, J. E. J. Bashucky, D. Kwok, N. Lee, A. D. Laforge, S. W. Cheong and K. S. Burch, *Appl. Phys. Lett.*, 2011, **98**, 141911.
17 M. Samanta and K. Biswas, *Chem. Mater.*, 2020, **32**, 8819–8826.
18 Y. Xia, D. Qian, D. Hsieh, L. Wray, A. Pal, H. Lin, A. Bansil, D. Grauer, Y. S. Hor, R. J. Cava and M. Z. Hasan, *Nat. Phys.*, 2009, **5**, 398–402.
19 Z.-H. Pan, E. Vescovo, A. V. Fedorov, D. Gsardner, Y. S. Lee, S. Chu, G. D. Gu and T. Valla, *Phys. Rev. Lett.*, 2011, **106**, 257004.
20 M. K. Jana, K. Biswas and C. N. R. Rao, *Chem. – Eur. J.*, 2013, **19**, 9110–9113.
21 M. Hong, Z. G. Chen, L. Yang, G. Han and J. Zou, *Adv. Electron. Mater.*, 2015, **1**, 1500025.
22 P. S. Maiti, S. Ghosh, G. Leitus, L. Houben and M. Bar Sadan, *Chem. Mater.*, 2021, **33**, 7558–7565.
23 D. Huo, G. Lin and M. Lv, *RSC Adv.*, 2022, **12**, 15150–15157.
24 M. Baitimirova, J. Andzane, G. Petersons, R. Meija, R. Poplausks, M. Romanova and D. Erts, *J. Mater. Sci.*, 2016, **51**, 8224–8232.
25 Z. Wang and S. Law, *Cryst. Growth Des.*, 2021, **21**, 6752–6765.
26 J. Andzane, L. Britala, E. Kauranens, A. Neciporenko, M. Baitimirova, S. Lara-Avila, S. Kubatkin, M. Bechelany and D. Erts, *Sci. Rep.*, 2019, **9**, 4791.
27 Y. Abusa, P. Yox, S. D. Cady, G. Viswanathan, J. Opare-Addo, E. A. Smith, Y. Mudryk, O. I. Lebedev, F. A. Perras and K. Kovnir, *J. Am. Chem. Soc.*, 2023, **145**, 22762–22775.
28 Y. Abusa, P. Yox, G. Viswanathan, J. Opare-Addo, A. Sarkar, V. Kyveryga, E. Smith, O. I. Lebedev and K. Kovnir, *J. Am. Chem. Soc.*, 2024, **146**(16), 11382–11391.
29 Y. Sun, H. Cheng, S. Gao, Q. Liu, Z. Sun, C. Xiao, C. Wu, S. Wei and Y. Xie, *J. Am. Chem. Soc.*, 2012, **134**, 20294–20297.

